



# Facet-dependent performance of anatase $\text{TiO}_2$ for photocatalytic oxidation of gaseous ammonia



Min Chen <sup>a,b</sup>, Jinzhu Ma <sup>a,b,c</sup>, Bo Zhang <sup>a,b</sup>, Fei Wang <sup>a,b</sup>, Yaobin Li <sup>a,b,c</sup>, Changbin Zhang <sup>a,b,\*</sup>, Hong He <sup>a,b,c</sup>

<sup>a</sup> State Key Joint Laboratory of Environment Simulation and Pollution Control, Research Center for Eco-Environmental Sciences, Chinese Academy of Sciences, Beijing 100085, China

<sup>b</sup> University of Chinese Academy of Sciences, Beijing 100049, China

<sup>c</sup> Center for Excellence in Regional Atmospheric Environment, Institute of Urban Environment, Chinese Academy of Sciences, Xiamen 361021, China

## ARTICLE INFO

### Article history:

Received 28 November 2016

Received in revised form 27 March 2017

Accepted 5 April 2017

Available online 6 April 2017

### Keywords:

Photocatalysis

$\text{TiO}_2$

Exposed facets

Charges separation

$\text{NH}_3$  oxidation

## ABSTRACT

Photocatalytic oxidation of gaseous ammonia ( $\text{NH}_3$ ) at room temperature is an efficient method for the elimination of  $\text{NH}_3$  emitted from indoor and outdoor sources, such as decorative materials, intensive livestock farming, chemical processes, etc. Herein, we prepared the anatase  $\text{TiO}_2$  with clean dominant  $\{001\}$ ,  $\{101\}$  and  $\{010\}$  facets, and tested their photocatalytic activity for  $\text{NH}_3$  oxidation. The test results show that the photocatalytic activity order for  $\text{NH}_3$  oxidation is revealed as  $\{001\} > \{101\} > \{010\}$ . The catalysts were characterized by XRD, FE-SEM, XPS, UV-vis, in situ DRIFTS and TPD methods. It is indicated that  $\text{TiO}_2$  with dominant  $\{001\}$  facets has the highest separation efficiency of the photogenerated charges among three catalysts. Since the photogenerated holes is responsible for initiating the first step of  $\text{NH}_3$  oxidation, the  $\text{TiO}_2$  with dominant  $\{001\}$  facets demonstrated the exceptional activity. In addition, the photocatalytic oxidation of  $\text{NH}_3$  possibly follow the photo-iSCR mechanism. The photogenerated electrons activate  $\text{O}_2$  and then participate in the formation of reactive intermediate  $\text{NO}_x$  followed by the photo- $\text{NH}_3$ -iSCR to final products. The present study will improve our understanding about the performance of anatase  $\text{TiO}_2$  for photocatalytic oxidation of  $\text{NH}_3$ .

© 2017 Elsevier B.V. All rights reserved.

## 1. Introduction

Gaseous ammonia ( $\text{NH}_3$ ) as one of the major air pollutants mainly stems from agriculture emissions and the release of decorative materials containing urea or ammonia compound-based antifreeze admixtures [1–4]. Excessive emissions of ammonia would give rise to a series of negative influences on environment and human health. Therefore, in order to meet the environmental regulations and health needs, it is necessary to develop the techniques for  $\text{NH}_3$  removal. Traditional techniques, such as selective catalytic oxidation (SCO), can effectively remove  $\text{NH}_3$ . A number of catalysts such as Cu and Fe exchanged ZSM-5 [5,6],  $\text{Ag}/\text{Al}_2\text{O}_3$  showed excellent SCO performance [7,8]. However, SCO of  $\text{NH}_3$  often performed at high temperature ( $>433\text{ K}$ ).

Since the discovery of photocatalytic splitting of water on  $\text{TiO}_2$  in 1972,  $\text{TiO}_2$  has been undoubtedly proven to be one of the best photocatalysts for pollutant removal due to its physical and chemical stability, low cost, easy availability, and unique electronic and optical properties [9–12]. Recently, the potential of photocatalytic elimination of  $\text{NH}_3$  at room temperature has already been well recognized [13–16]. Yamazoe et al. compared the activity of photocatalytic oxidation of  $\text{NH}_3$  (PCO) over various commercial  $\text{TiO}_2$  [14]. In our previous study, we found that fluorine modified  $\text{TiO}_2$  showed the excellent activity for PCO of  $\text{NH}_3$  [17].

Since the synthesis of anatase  $\text{TiO}_2$  with high percentage of  $\{001\}$  facets exposed was firstly reported by Lu et al. [18], facet-dependent photocatalytic properties of anatase  $\text{TiO}_2$  nanocrystals with well-defined facets have received enormous research attention [19–26]. Generally,  $\{101\}$ ,  $\{001\}$  and  $\{010\}$  facets are the three fundamental low-index facets of anatase  $\text{TiO}_2$  crystals. The results of theoretically calculated surface energy showed that the surface energy of anatase  $\text{TiO}_2$  increases in the order of  $\{101\}$  facet ( $0.44\text{ J}\cdot\text{m}^{-2}$ )  $<$   $\{010\}$  facet ( $0.53\text{ J}\cdot\text{m}^{-2}$ )  $<$   $\{001\}$  facet ( $0.90\text{ J}\cdot\text{m}^{-2}$ ) [18]. Han et al. [27] found that  $\{001\}$  facets showed superior photodegradative activity for organic pollutants, while Pan et al. [19]

\* Corresponding author at: State Key Joint Laboratory of Environment Simulation and Pollution Control, Research Center for Eco-Environmental Sciences, Chinese Academy of Sciences, Beijing 100085, China.

E-mail address: [cbzhang@rcees.ac.cn](mailto:cbzhang@rcees.ac.cn) (C. Zhang).

pointed out that {010} or {101} facet of  $\text{TiO}_2$  exhibited higher photoreactivity than {001} facets for the  $\text{H}_2$  evolution reaction. Besides, {010} facet exposed anatase  $\text{TiO}_2$  was demonstrated to be superior to {101} and {001} facets for the  $\text{CO}_2$  reduction by Ye et al. [28]. Apparently, the activity order for the different facets of anatase  $\text{TiO}_2$  is closely related to the photocatalytic reaction type.

There are three main factors influencing the activity of anatase  $\text{TiO}_2$  with well-defined facets. (i) The different exposed facets have distinct band structure, which determine the separation efficiency of the photogenerated carriers in a photocatalytic reaction. Generally, the wider the band gap a semiconductor associate with the higher quantum efficiency [10]. (ii) The difference of preferential transport directions of photogenerated carriers with regard to the facet-dependent photocatalytic activity is believed to be an important factor. It was documented that {001} facets favor to trap holes as oxidative sites, while {101} facets incline to trap electrons as reductive sites [29,30]. (iii) A specific photocatalytic reaction has its own features, for example,  $\text{CO}_2$  reduction should need more strongly reductive electrons [28], however, for many organic pollutants degradation, photogenerated holes direct oxidation or  $\cdot\text{OH}$  indirect oxidation play a dominant role [31,32]. The activity order of a specific photocatalytic reaction over different exposed facet of anatase  $\text{TiO}_2$  is determined by the combined effect of above factors.

In the present study, dominant {001}, {101}, {010} facet exposed anatase  $\text{TiO}_2$  were controllably synthesized and were applied to the PCO of  $\text{NH}_3$  under room temperature. Based on the results of XRD, SEM, XPS, UV-vis, DRIFTS and TPD characterization, the relationship between facet-dependent physic-chemical properties of  $\text{TiO}_2$  and the performance of  $\text{NH}_3$  oxidation was explored.

## 2. Experimental

### 2.1. Preparation of catalysts

**T001:**  $\text{TiO}_2$  with exposed {001} facets (denoted as T001) was controllably prepared according to a modified HF hydrothermal method similar to that reported by Han et al. [27]. In a typical synthesis, 4 mL of hydrofluoric acid solution (40 wt.%) was added dropwise into the prepared  $\text{Ti}(\text{OC}_4\text{H}_9)_4$  (25 mL) in a 100 mL Teflon-lined autoclave at room temperature under magnetic stirring, then the autoclave was sealed and heated at 190 °C for 24 h. After hydrothermal reaction, the white precipitate was collected and washed with ethanol and distilled water several times, then dried overnight in an oven at 60 °C and finally 550 °C calcination for 2 h.

**T101:** {101} facet exposed  $\text{TiO}_2$  (denoted as T101) were synthesized by a two-step hydrothermal procedure similar to previous reports [24]. In the first step, 1 g of P25 was reacted hydrothermally with 70 mL KOH solution (10 M) in a Teflon-lined autoclave with a capacity of 100 mL at 200 °C for 48 h. The resulting precipitate was washed and neutralized using deionized water and dried at 60 °C. In the second step, the prepared potassium titanate (70 mg) was stirred in distilled water (70 mL) and heated in a 100 mL Teflon-lined autoclave at 170 °C for 24 h. The white precipitate was washed and dried at 100 °C.

**T010:** the route was similar to that of the T101 sample except that the second hydrothermal temperature was 200 °C.

### 2.2. Characterization

The crystalline structure of the photocatalysts was examined by powder X-ray diffractometer (XRD; X'Pert PRO, PANalytical, Netherlands) with  $\text{Cu K}\alpha$  ( $\lambda = 0.15406 \text{ nm}$ ) radiation at 40 kV and 40 mA. The patterns were collected over the  $2\theta$  range from 10° to 90° with a scan step of 0.02°. The morphology of the photocatalysts were investigated using a SU8000 field emission scanning elec-

tron microscope (FE-SEM). The powder of a sample was deposited on a silicon wafer before FE-SEM measurements. The specific surface area was obtained at 77 K over the whole range of relative pressures, using a Quantachrome Quadsorb SI-MP analyzer. The catalysts were degassed at 300 °C for 3 h prior to the  $\text{N}_2$  physisorption. The BET equation was applied to calculate the Specific surface areas in the 0.05–0.3 partial pressure range from the adsorption isotherm. X-ray photoelectron spectroscopy (XPS) was measured on a Scanning X-ray Microprobe (AXIS Ultra, Kratos Analytical, Inc.), and the spectra were calibrated to the C 1s peak at 284.6 eV. The UV-vis diffuse reflection spectra (DRS) were obtained in air with  $\text{Al}_2\text{O}_3$  as a reference with a diffuse reflectance UV-vis Spectrophotometer (U-3310, Hitachi).

The photochemical properties of the photocatalysts was investigated by in situ diffuse reflectance infrared Fourier transform spectroscopy (DRIFTS). A Fourier transform infrared spectrometer (Nicolet 380) equipped with a MCT detector was used to collect the infrared spectra, a spectra range from 4000 to 800  $\text{cm}^{-1}$  with a resolution of 4  $\text{cm}^{-1}$ . The reaction cell has three windows, where two are ZnSe windows used for entry and exit of the detection infrared beam. The third quartz window is for the transmission of UV light during in situ photoreactions.

### 2.3. PCO activity tests

The photocatalytic activity tests for the oxidation of  $\text{NH}_3$  were performed in a home-made flow reactor at ambient temperature. The stainless steel reactor was covered with a quartz plate. A round dish containing the photocatalyst was placed in the center of the reactor. 70 mg photocatalyst was dispensed on the round dish for each evaluation experiment. The light source is a 500 W commercial Hg lamp (Beijing TrusTech Science and Technology Co., China) with an optical filter ( $\lambda = 365\text{--}366 \text{ nm}$ ), and the average light intensity was 10.5 mW/cm<sup>2</sup>. The commercial Hg lamp was vertically placed outside the reactor, and the temperature of the photocatalyst was kept at 25 °C by water circulation. The concentrations of effluent gas, including  $\text{NH}_3$ ,  $\text{NO}$ ,  $\text{NO}_2$  and  $\text{N}_2\text{O}$ , were measured by an FTIR spectrometer (Nicolet 380) equipped with 2 m gas cell and a DTGS detector. The reactant gas circularly flowed over the catalyst, and the volume of reactant gas was about 1.5 L and the initial concentration of reactant gas was 500 ppm  $\text{NH}_3$ , 20 vol%  $\text{O}_2$ , and  $\text{N}_2$  balance.

## 3. Results and discussion

### 3.1. Structure characterization

The crystallographic structure of the as-synthesized samples was confirmed by the X-ray diffraction patterns (XRD). As shown in Fig. 1, the samples all show the peaks located at 25.28°, 36.95°, 37.8°, 38.58°, 48.05°, 53.89°, 55.96°, 62.69°, 68.76°, 70.31°, and 75.03°, which are indexed to {101}, {103}, {004}, {112}, {200}, {105}, {211}, {204}, {116}, {220}, and {215} facet of tetragonal anatase  $\text{TiO}_2$  (JCPDS No. 21-1272), demonstrating that the synthesized T001, T101, and T010 are pure anatase  $\text{TiO}_2$ . Moreover, no typical peaks of other  $\text{TiO}_2$  polymorph such as brookite or rutile were observed. Specific surface area (SSA) of T001, T101, and T010 are 84  $\text{m}^2/\text{g}$ , 41  $\text{m}^2/\text{g}$  and 27  $\text{m}^2/\text{g}$ , respectively.

The morphology of as-prepared catalysts was characterized by FE-SEM and the images are shown in Fig. 2. The T001 displays the typical nanosheet morphology with a length from 40 to 60 nm and a thickness of about 8 nm. The obtained T101 is mainly composed of octahedral bipyramids, and the average side length of the bipyramids is about 80 nm. T010 shows nanorods morphology with size of about 300 nm × 50 nm. According to the reported method [24],

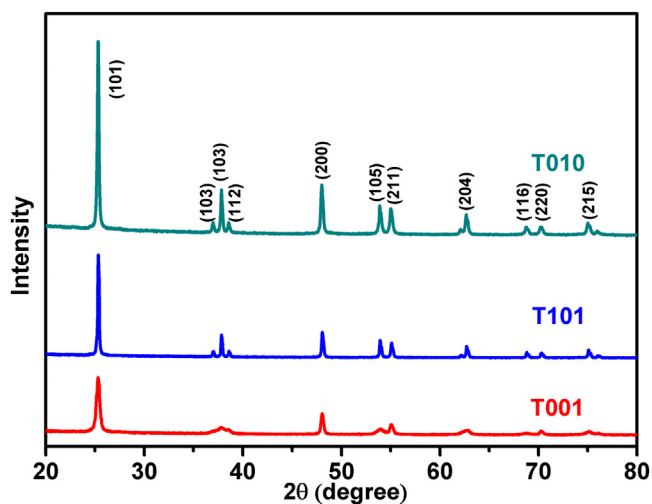


Fig. 1. XRD patterns of the T001, T101, and T010.

**Table 1**  
Physiochemical Properties of T001, T101, and T010.

Sample	Morphology	SSA ( $\text{m}^2/\text{g}$ )	Crystal size (nm)	Predominant facet (%)
T001	nanosheets	84	15.9	68.7
T101	nanocahedra	41	48.8	90.2
T010	nanorod	27	60.4	83.3

the areas of each facet and total surface area were calculated based on FE-SEM images, and then the percentage of each predominant facet was obtained through dividing the total surface area by the area of {001}, {101} and {010} facets. As shown in Table 1, the percentages of {001}, {101}, and {010} are 68.7%, 90.2% and 83.3%, respectively.

The X-ray photoelectron spectra (XPS) were measured to analyze the surface chemical composition of the samples. Fig. 3a shows the XPS survey spectra of the T001, T101, and T010. The three samples all contain Ti, O, and C elements with sharp photoelectron peaks at binding energies of 458 eV (Ti2p), 531 eV (O1s), and 285 eV (C1s). The residual carbon from samples and hydrocarbon from the XPS instrument itself attributed to the carbon peak. Considering that hydrofluoric acid was used as a shape controlling agent in the synthesis of T001, in order to exclude the effects of surface fluorine [17], high temperature calcination was carried out to remove surface fluorine. XPS spectrum (Fig. 3b) showed that no F1s peak at 684 eV attributed to the formation of  $\equiv\text{Ti}=\text{F}$  exist, confirming the absence of surface fluorine [17,33]. Therefore, we successfully synthesized the clean predominant  $\text{TiO}_2$  with {001}, {101}, and {010} facets exposed.

### 3.2. PCO of $\text{NH}_3$ performance

T001, T101, and T010 were next tested for the PCO of  $\text{NH}_3$ . The reaction of  $\text{NH}_3$  oxidation was negligible when control experiments were performed under UV irradiation in the absence of photocatalyst. Before UV irradiation, the catalyst- $\text{NH}_3$  flows were kept in dark for 2 h to reach the  $\text{NH}_3$  adsorption-desorption equilibrium on the surface of catalyst. Fig. 4a plotted the  $\text{C}/\text{C}_0$  with irradiation time, where “ $\text{C}_0$ ” and “ $\text{C}$ ” are the  $\text{NH}_3$  concentration before and after UV irradiation, respectively. We found that an excellent linear relationship between  $\log(\text{C}/\text{C}_0)$  and irradiation time (Fig. 4b), indicating that the PCO of  $\text{NH}_3$  follows a pseudo-first-order kinetic. The results show that the photocatalytic activity order is T001 > T101 > T010. Specifically, T001 exhibited the highest PCO of  $\text{NH}_3$  activity among three samples and its  $k$  reached  $0.034 \text{ min}^{-1}$ , which is 8.5 and 34

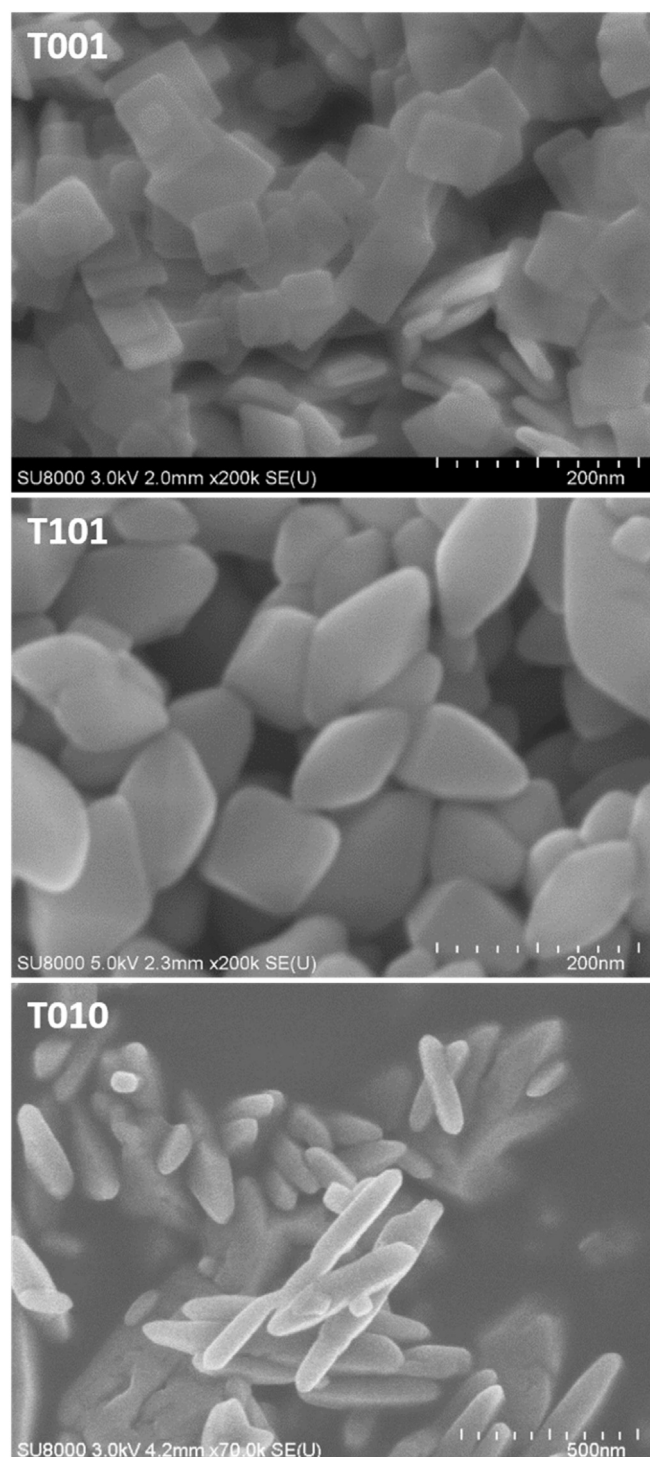


Fig. 2. SEM images of the T001, T101, and T010.

times higher than that of T101 and T010, respectively. Considering the effect of surface area, the rate constants were next normalized with the surface area, and the specific rate constant of T001 is 4.1 and 8.4 times as high as that of T101 and T010.

In addition, reliability and stability of a catalyst are very important for applications of photocatalysts. To evaluate this, repeated activity tests of T001 were carried out at regular intervals and the results are shown in Fig. 5. A relative stable  $\text{NH}_3$  conversion was observed for four cycles without an apparent decrease, demonstrating the high stability of T001 photocatalyst.

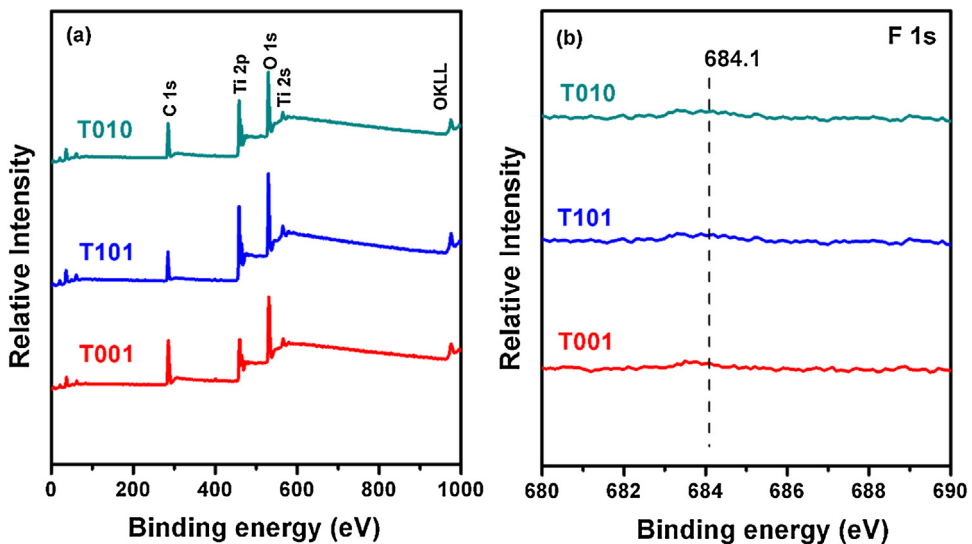


Fig. 3. XPS survey spectra (a) and high resolution XPS spectra of F 1s (b) of T001, T101, and T010.

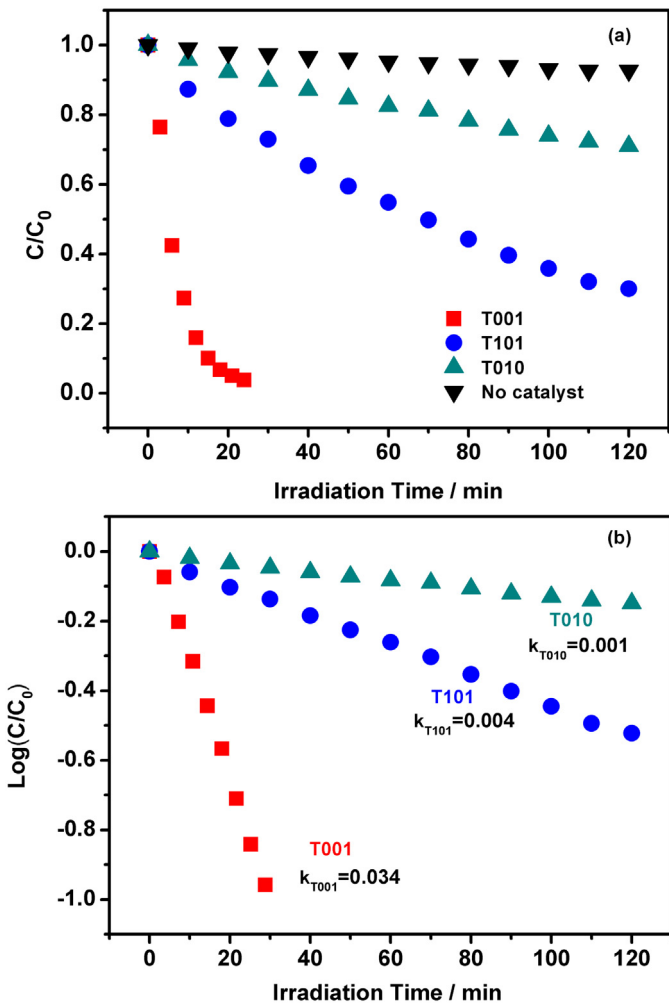


Fig. 4. Photocatalytic oxidation of  $\text{NH}_3$   $C/C_0$  vs reaction time (a) and rate constants compare under UV irradiation over T001, T101, and T010 (b).

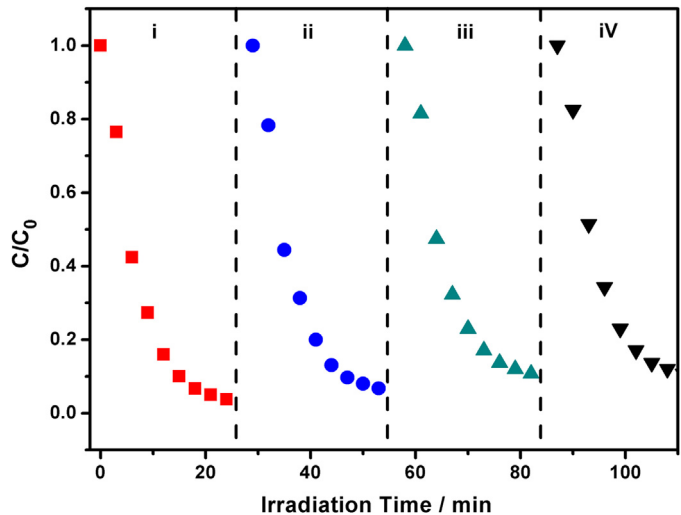


Fig. 5. Reusability of the T001 in four successive experimental runs for photocatalytic oxidation of  $\text{NH}_3$ .

### 3.3. Reason analyses of the activity order for PCO of $\text{NH}_3$

#### 3.3.1. Photochemical properties

The electronic structure is an important factor for the photocatalytic activity of anatase  $\text{TiO}_2$ . Valence band (VB) and conduction band (CB) energy levels determine the redox potentials and the separation efficiency of the photogenerated carriers in a photocatalytic reaction [19,34]. Therefore, we investigated the electronic structures of the T001, T101, and T010. UV-vis absorption spectra (Fig. 6a) show that the absorption edge of T001 has an obvious redshift compared with T101 and T010, and the bandgaps of T001, T101, and T010 were calculated to be a value of approximately 3.23, 3.27, and 3.29 eV, respectively. Fig. 6b shows the X-ray photoelectron valence band spectra of the samples. The VB maxima of all three anatase  $\text{TiO}_2$  crystals are at about 1.9 eV below the Fermi energy, which is consistent with the previous reports [34,35]. Then it can be induced that the CB minimum of T101 and T010 rise in contrast to T001, and the band structures of T001, T101, and T010 are illustrated in Fig. 6c. Pan et al. [19] pointed out that {101} and {010} facet exposed anatase  $\text{TiO}_2$  should have superior photoreactivity to {001} facet, because more strongly reductive electrons can

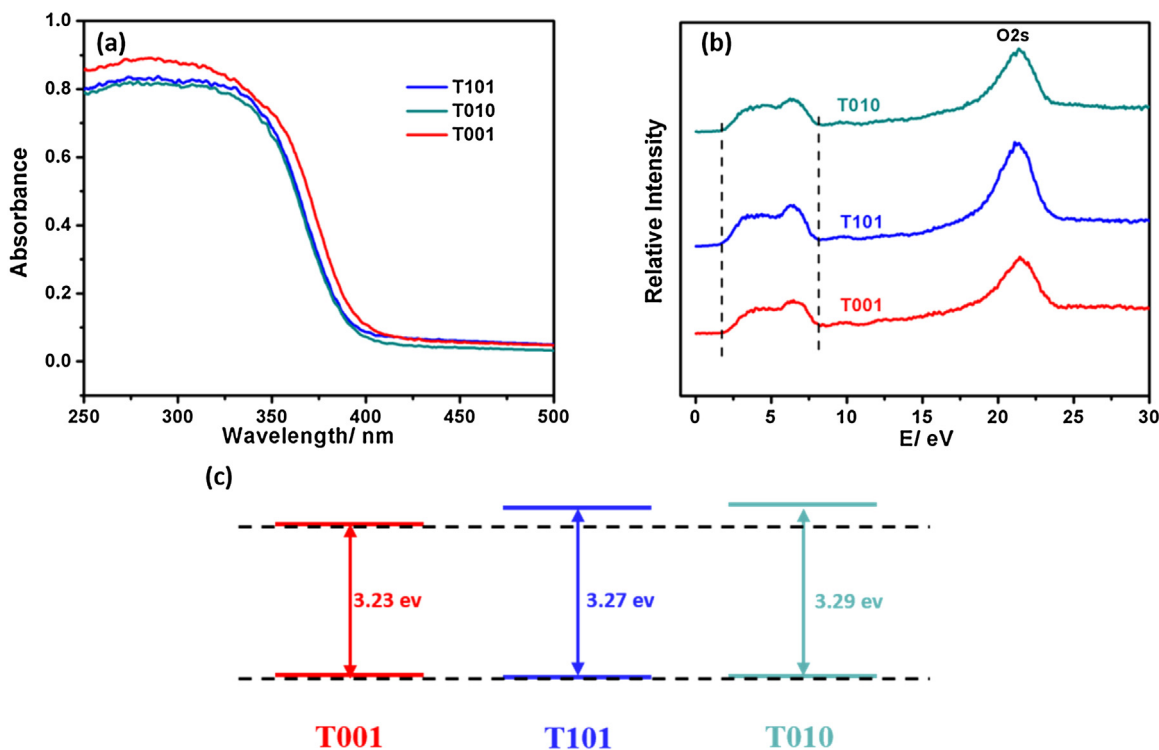


Fig. 6. UV/Vis absorption spectra of T001, T101, and T010 (a). VB XPS spectra of T001, T101, and T010. (b) VB and CB edges of T001, T101, and T010 (c).

be generated on {101} and {010} facets with a higher CB minimum. Active oxidizing species such as  $\bullet\text{O}_2^-$  and  $\bullet\text{OH}$  can be produced via the reduction of  $\text{O}_2$  by the CB electrons, then the organic pollutants can be well oxidized to  $\text{CO}_2$ ,  $\text{H}_2\text{O}$  and other products. However, we found that T101 and T010 exhibited worse performance to that of T001 in our activity tests (Fig. 5), it is therefore possible that photogenerated electrons is not very effective for the PCO of  $\text{NH}_3$ . Ye et al. [28] also found that {101} and {010} facets exposed  $\text{TiO}_2$  exhibited poor activity in dye degradation compared with {001} facets exposed  $\text{TiO}_2$ , which may be accounted for in a similar way.

Photogenerated holes on VB band transfer to surface adsorbed  $\text{H}_2\text{O}$  or  $\text{OH}^-$ , initiating photooxidation reactions, is another extremely important step in the photocatalytic process and possibly plays a key role in the PCO of  $\text{NH}_3$  [36–41]. Therefore, we next investigated the migration of photogenerated holes by in situ DRIFTS method using  $\text{H}_2\text{O}$  oxidation as a probe reaction. Infrared spectroscopy is very sensitive to the decrease or increase of surface  $\text{H}_2\text{O}$  and the accumulation of electrons on the  $\text{TiO}_2$  surface resulting from  $\text{H}_2\text{O}$  oxidation by holes can usually absorb mid-IR (MIR) light and thus is able to be monitored by IR spectroscopy [42–45]. As shown in Fig. 7, in the absence of redox species except for  $\text{H}_2\text{O}$ , the UV irradiation caused no change in the IR spectra of T101 and T010, indicating that  $\text{H}_2\text{O}$  oxidation has not occurred and further demonstrating the repaid electron-hole pairs recombination on T101 and T010. However, in the case of the T001, the UV irradiation triggered an obvious increase in the background IR absorbance band ranging from 3000 to 1000  $\text{cm}^{-1}$ , which is attributed to electron accumulation in the conduction band. Besides, a broad negative absorption band ranging from 3700 to 3000  $\text{cm}^{-1}$  and narrow negative peak at 1628  $\text{cm}^{-1}$  appeared, which were assigned to  $\nu(\text{OH})$  and  $\delta(\text{H}_2\text{O})$ , respectively. These results revealed that the surface adsorbed  $\text{H}_2\text{O}$  on T001 is effectively oxidized by photogenerated holes under UV irradiation, demonstrating that the electron-hole pairs are well separated over T001 and more photogenerated holes were driven to the surface to oxidize the  $\text{H}_2\text{O}$ , which should be the main reason why T001 is much more active than T101 and T010 for the PCO of

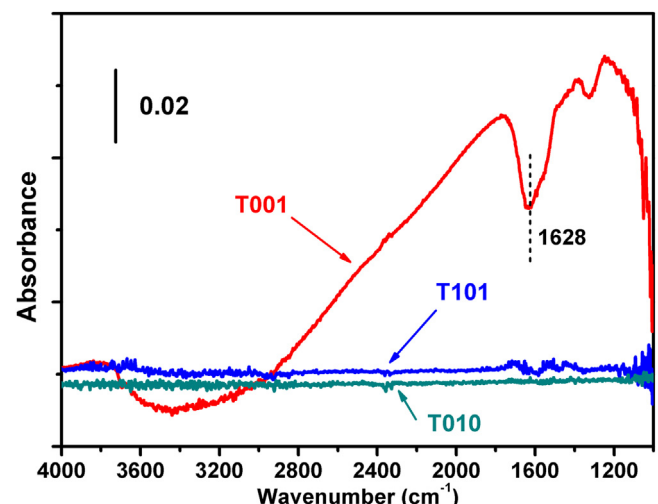


Fig. 7. IR spectra of T001, T101, and T010 after 5 min UV irradiation under  $\text{N}_2$  atmosphere.

$\text{NH}_3$ . In addition, previous studies have reported that {001} facets exposed anatase  $\text{TiO}_2$  favor to trap holes as oxidative sites while {101} facets incline to trap electrons as reductive sites by electron spin resonance (ESR) or single molecule fluorescence probe methods [29,30]. Since our DRIFTS are carried out at room temperature, the present characterization of photogenerated charges should be more appropriate than low temperature ESR technique.

### 3.3.2. The reaction mechanism for PCO of $\text{NH}_3$

We firstly investigated the role of  $\text{O}_2$  in the PCO of  $\text{NH}_3$ . On one hand,  $\text{O}_2$  as an electron-capture to produce  $\bullet\text{O}_2^-$ , is beneficial to the separation of photogenerated  $\text{e}^-$  and  $\text{h}^+$ ; on the other hand,  $\text{O}_2$  can be an oxidant participating in the oxidation of substrate such as organic dyes. As shown in Fig. 8,  $\text{NH}_3$  can be steadily removed

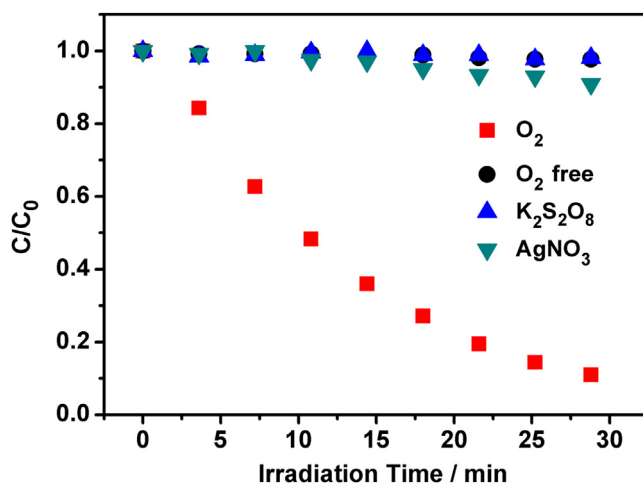


Fig. 8. Activity tests for photocatalytic oxidation of  $\text{NH}_3$  in the presence of different electron-captures.

over T001 in the case of the co-existence presence of  $\text{NH}_3$  and  $\text{O}_2$ . However,  $\text{NH}_3$  was not oxidized in the absence of  $\text{O}_2$  possibly due to the combination of photogenerated  $e^-$  and  $h^+$ . When  $\text{O}_2$  was replaced by  $\text{AgNO}_3$  or  $\text{K}_2\text{S}_2\text{O}_8$  which are common used electron-captures, still no activity of PCO of  $\text{NH}_3$  was observed even though the photogenerated  $e^-$  and  $h^+$  are well separated. These results reveals that only efficient separation of photogenerated charges on the  $\text{TiO}_2$  surface is not enough for realizing the  $\text{NH}_3$  oxidation. As reported, the initial step of  $\text{NH}_3$  oxidation is that the  $\text{NH}_3$  is activated by a photogenerated hole to produce the amino radical ( $^{\bullet}\text{NH}_2$ ) [46]. However, if  $\text{O}_2$  does not participate in the subsequent oxidation of  $^{\bullet}\text{NH}_2$ ,  $\text{NH}_3$  oxidation would be terminated.

The reaction products of PCO of  $\text{NH}_3$  in our flow system was also investigated. The products analysis on T001 (Fig. 9a) shows that no  $\text{NO}_x$  was detected and only 7 ppm  $\text{N}_2\text{O}$  were produced. Very recently, Raff et al. [47,48] reported that the oxidation of low concentration of  $\text{NH}_3$  oxidation (ppb level) over  $\text{TiO}_2$  will lead to the relative high yields of  $\text{NO}_x$ . Therefore, we deduced that the mechanism of high concentration of  $\text{NH}_3$  oxidation might be different from the low concentration of  $\text{NH}_3$  oxidation. We further analyzed the surface products over the T001 by TPD measurement after activity tests. As shown in Fig. 9b, a broad  $\text{NO}$  peak in the range of 250–340 °C and a weak  $\text{NO}_2$  peak in the range of 150–300 °C appeared, which ascribe to the desorption of  $\text{NO}_x$  species ( $\text{NO}_2^-$  and  $\text{NO}_3^-$ ) formed over catalyst surface during the PCO of  $\text{NH}_3$  [49]. Then it is indicated that  $\text{NO}_x$  is possibly the reactive intermediate products and then is active to be reactive with surface  $\text{NH}_2$  to generate  $\text{N}_2$ .

Based on the above results, we propose that the reaction mechanism probably follows the photo-iSCR mechanism and is shown in Fig. 10. When  $\text{TiO}_2$  is excited by UV irradiation, the electron-hole charge carriers are produced and then migrate to the surface of  $\text{TiO}_2$  (step 1). Photogenerated holes initiate the  $\text{NH}_3$  oxidation on the surface of  $\text{TiO}_2$ , which results in formation of the  $^{\bullet}\text{NH}_2$  (step 2). In the following step (step 3),  $^{\bullet}\text{NH}_2$  react with active oxygen species such as  $^{\bullet}\text{O}_2^-$  and  $^{\bullet}\text{OH}$  to generate the intermediate  $\text{NO}_x$ . Finally, the in situ formed  $\text{NO}_x$  is to be reduced by  $^{\bullet}\text{NH}_2$  to produce  $\text{N}_2$  or  $\text{N}_2\text{O}$  (step 4). The predominant {001} facets exposed  $\text{TiO}_2$  has the higher hole migration compared with predominant {101} or {010} facets exposed  $\text{TiO}_2$ , then the kinetics rate of step 2 can be enhanced. Moreover, since the separation of photogenerated  $e^-$  and  $h^+$  is efficient over T001, more photogenerated  $e^-$  will be available to produce more active oxygen species, beneficial to step 3. Evidently, the T001 demonstrated the much high activity for the PCO of  $\text{NH}_3$  oxidation (Fig. 4).

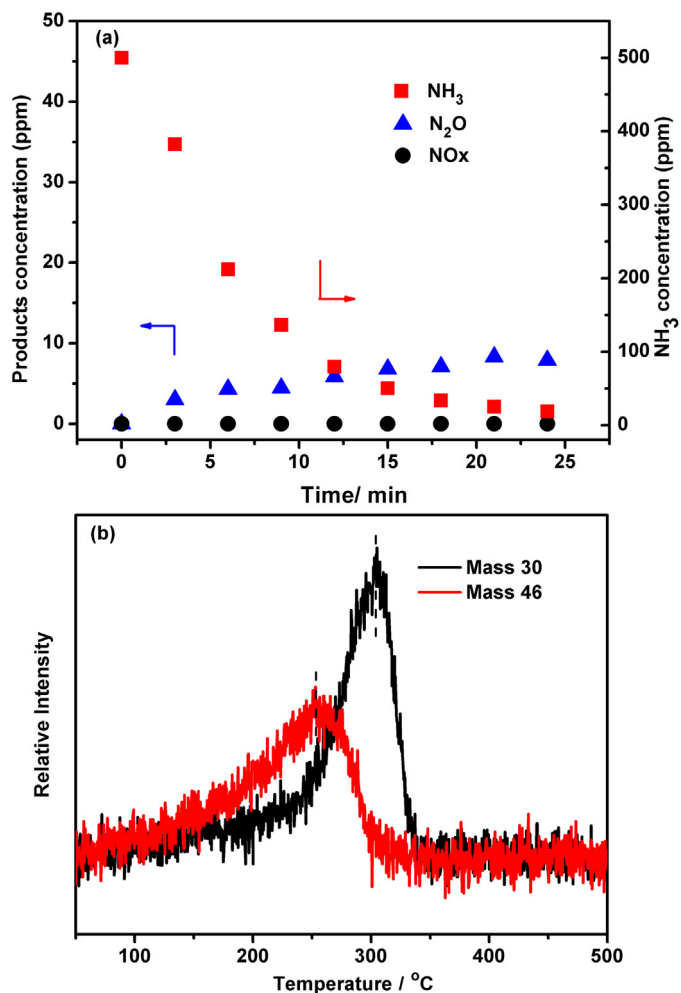


Fig. 9. Gaseous products analysis of photocatalytic oxidation of  $\text{NH}_3$  on T001 (a). Surface products of  $\text{NH}_3$  oxidation on T001 (b).

#### 4. Conclusions

In summary, anatase  $\text{TiO}_2$  nanoparticles with dominant {001}, {101}, and {010} facets exposed were successfully synthesized via the hydrothermal method. The photocatalytic activity order for  $\text{NH}_3$  oxidation of is {001} > {101} > {010}.  $\text{TiO}_2$  with dominant {001} facets allows more photogenerated holes to trap on its surface and therefore shows the highest efficiency for the separation of photogenerated electron-hole pairs among three catalysts. Since the photogenerated holes play a key role in the PCO of  $\text{NH}_3$ , the T001 showed much higher activity than T101 and T010. The photogenerated electrons could activate  $\text{O}_2$  species and then participate in the formation of reactive intermediate  $\text{NO}_x$  followed by the photo- $\text{NH}_3$ -iSCR to final products.

#### Acknowledgments

This work was financially supported by the National Natural Science Foundation of China (21422706, 21577159), the Strategic Priority Research Program of the Chinese Academy of Sciences (XDB05050600) and the Youth Innovation Promotion Association, CAS (2017064).

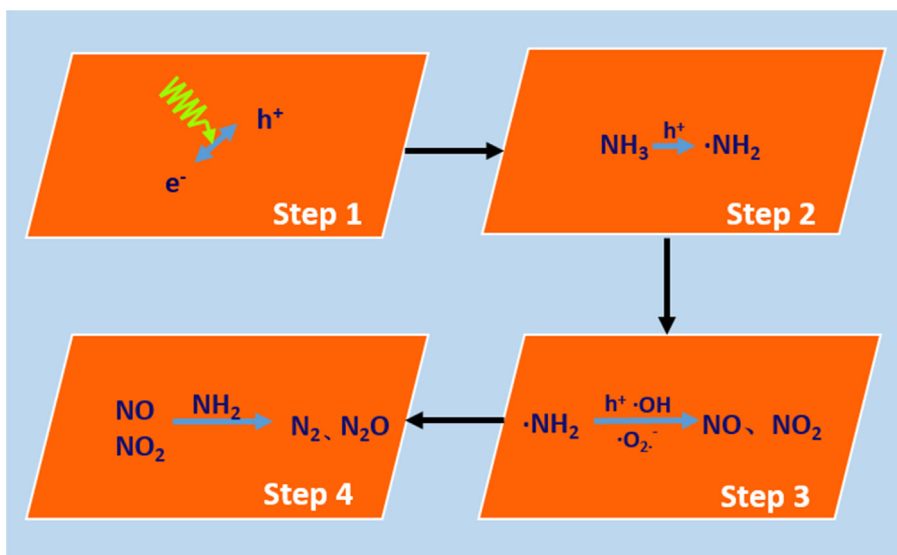


Fig. 10. Possible reaction mechanism of photocatalytic oxidation of  $\text{NH}_3$  over  $\text{TiO}_2$ .

## References

- [1] Y. Dong, Z. Bai, R. Liu, T. Zhu, *Atmos. Environ.* 41 (2007) 3182–3192.
- [2] Y. Huang, S.C. Lee, K.F. Ho, S.S.H. Ho, N. Cao, Y. Cheng, Y. Gao, *Atmos. Environ.* 59 (2012) 224–231.
- [3] S. Wang, J. Xing, C. Jang, Y. Zhu, J.S. Fu, J. Hao, *Environ. Sci. Technol.* 45 (2011) 9293–9300.
- [4] F. Zhou, P. Ciais, K. Hayashi, J. Galloway, D.G. Kim, C. Yang, S. Li, B. Liu, Z. Shang, S. Gao, *Environ. Sci. Technol.* 50 (2016) 564–572.
- [5] R.Q. Long, R.T. Yang, *Chem. Commun.* (2000) 1651–1652.
- [6] R.Q. Long, R.T. Yang, *J. Catal.* 201 (2001) 145–152.
- [7] L. Zhang, C. Zhang, H. He, *J. Catal.* 261 (2009) 101–109.
- [8] L. Zhang, H. He, *J. Catal.* 268 (2009) 18–25.
- [9] M.R. Hoffmann, S.T. Martin, W.Y. Choi, D.W. Bahnemann, *Chem. Rev.* 95 (1995) 69–96.
- [10] X. Chen, S.S. Mao, *Chem. Rev.* 107 (2007) 2891–2959.
- [11] A. Fujishima, X. Zhang, D. Tryk, *Surf. Sci. Rep.* 63 (2008) 515–582.
- [12] G. Liu, H.G. Yang, J. Pan, Y.Q. Yang, G.Q. Lu, H.M. Cheng, *Chem. Rev.* 114 (2014) 9559–9612.
- [13] S. Heylen, S. Smet, K.G.M. Laurier, J. Hofkens, M.B.J. Roeffaers, J.A. Martens, *Catal. Sci. Technol.* 2 (2012) 1802–1805.
- [14] S. Yamazoe, T. Okumura, T. Tanaka, *Catal. Today* 120 (2007) 220–225.
- [15] P.A. Kolinko, D.V. Kozlov, *Appl. Catal. B* 90 (2009) 126–131.
- [16] H. Wang, Y. Su, H. Zhao, H. Yu, S. Chen, Y. Zhang, X. Quan, *Environ. Sci. Technol.* 48 (2014) 11984–11990.
- [17] H. Wu, J. Ma, Y. Li, C. Zhang, H. He, *Appl. Catal. B* 152–153 (2014) 82–87.
- [18] H.G. Yang, C.H. Sun, S.Z. Qiao, J. Zou, G. Liu, S.C. Smith, H.M. Cheng, G.Q. Lu, *Nature* 453 (2008) 638–641.
- [19] J. Pan, G. Liu, G.Q. Lu, H.M. Cheng, *Angew. Chem. Int. Ed.* 50 (2011) 2133–2137.
- [20] F. Amano, T. Yasumoto, O.O. Prieto-Mahaney, S. Uchida, T. Shibayama, B. Ohtani, *Chem. Commun.* (2009) 2311–2313.
- [21] T.R. Gordon, M. Cargnello, T. Paik, F. Mangolini, R.T. Weber, P. Fornasiero, C.B. Murray, *J. Am. Chem. Soc.* 134 (2012) 6751–6761.
- [22] N. Roy, Y. Sohn, D. Pradhan, *ACS Nano* 7 (2013) 2532–2540.
- [23] N. Roy, Y. Park, Y. Sohn, K.T. Leung, D. Pradhan, *ACS Appl. Mater. Inter.* 6 (2014) 16498–16507.
- [24] C. Li, C. Koenigsmann, W. Ding, B. Rudshteyn, K.R. Yang, K.P. Regan, S.J. Konezny, V.S. Batista, G.W. Brudvig, C.A. Schmuttenmaer, J.H. Kim, *J. Am. Chem. Soc.* 137 (2015) 1520–1529.
- [25] L. Ye, J. Mao, J. Liu, Z. Jiang, T. Peng, L. Zan, *J. Mater. Chem. A* 1 (2013) 10532–10537.
- [26] C. Chen, G.A. Sewvandi, T. Kusunose, Y. Tanaka, S. Nakanishi, Q. Feng, *CrystEngComm* 16 (2014) 8885–8895.
- [27] X. Han, Q. Kuang, M. Jin, Z. Xie, L. Zheng, *J. Am. Chem. Soc.* 131 (2009) 3152–3253.
- [28] L. Ye, J. Mao, T. Peng, L. Zan, Y. Zhang, *Phys. Chem. Chem. Phys.* 16 (2014) 15675–15680.
- [29] M. D'Arienzo, J. Carbajo, A. Bahamonde, M. Crippa, S. Polizzi, R. Scotti, L. Wahba, F. Morazzoni, *J. Am. Chem. Soc.* 133 (2011) 17652–17661.
- [30] T. Tachikawa, S. Yamashita, T. Majima, *J. Am. Chem. Soc.* 133 (2011) 7197–7204.
- [31] M. Wang, F. Zhang, X. Zhu, Z. Qi, B. Hong, J. Ding, J. Bao, S. Sun, C. Gao, *Langmuir* 31 (2015) 1730–1736.
- [32] L. Ren, Y. Li, J. Hou, J. Bai, M. Mao, M. Zeng, X. Zhao, N. Li, *Appl. Catal. B* 181 (2016) 625–634.
- [33] Q. Xiang, K. Lv, J. Yu, *Appl. Catal. B* 96 (2010) 557–564.
- [34] X. Chen, C. Burda, *J. Am. Chem. Soc.* 130 (2008) 5018–5019.
- [35] F. Dong, W. Zhao, Z. Wu, S. Guo, J. Hazard. Mater. 162 (2009) 763–770.
- [36] T. Tachikawa, M. Fujitsuka, T. Majima, *J. Phys. Chem. C* 111 (2007) 5259–5275.
- [37] H. Fu, L. Zhang, S. Zhang, Y. Zhu, J. Zhao, *J. Phys. Chem. B* 110 (2006) 3061–3065.
- [38] H. Sheng, Q. Li, W. Ma, H. Ji, C. Chen, J. Zhao, *Appl. Catal. B* 138–139 (2013) 212–218.
- [39] M. Chen, K. Peng, H. Wang, Z. Yang, Q. Zeng, A. Xu, *Chem. Eng. J.* 197 (2012) 110–115.
- [40] D. Dvoranova, Z. Barberekova, V. Brezova, *Molecules* 19 (2014) 17279–17304.
- [41] J. Ma, C. Wang, H. He, *Appl. Catal. B* 184 (2016) 28–34.
- [42] S. Shen, X. Wang, T. Chen, Z. Feng, C. Li, *J. Phys. Chem. C* 118 (2014) 12661–12668.
- [43] H. Sheng, H. Zhang, W. Song, H. Ji, W. Ma, C. Chen, J. Zhao, *Angew. Chem. Int. Ed.* 54 (2015) 5905–5909.
- [44] D.A. Panayotov, S.P. Burrows, J.R. Morris, *J. Phys. Chem. C* 116 (2012) 4535–4544.
- [45] F. Guzman, S.S. Chuang, *J. Am. Chem. Soc.* 132 (2010) 1502–1503.
- [46] S. Yamazoe, K. Teramura, Y. Hitomi, T. Shishido, T. Tanaka, *J. Phys. Chem. C* 111 (2007) 14189–14197.
- [47] M.A. Kebede, M.E. Varner, N.K. Scharko, R.B. Gerber, J.D. Raff, *J. Am. Chem. Soc.* 135 (2013) 8606–8615.
- [48] M.A. Kebede, N.K. Scharko, L.E. Appelt, J.D. Raff, *J. Phys. Chem. Lett.* 4 (2013) 2618–2623.
- [49] R.V. Mikhaylov, A.A. Lisachenko, B.N. Shelimov, V.B. Kazansky, G. Martra, G. Alberto, S. Coluccia, *J. Phys. Chem. C* 113 (2009) 20381–20387.